Least Degree G^1-refinable Multi-sided Surfaces Suitable for Inclusion into C^1 bi-2 Splines

Kęstutis Karčiauskas[a], Jörg Peters[b,*]

Department CISE, University of Florida

[a] *Vilnius University, Lithuania*
[b] *University of Florida, USA*

Abstract

Geometrically smooth spline surfaces, generalized to include n-sided facets or configurations of $n \neq 4$ quads, can exhibit a curious lack of additional degrees of freedom for modelling or engineering analysis when refined.

This paper establishes a minimal polynomial degree for smooth constructions of multi-sided surfaces that guarantees more flexibility in all directions under refinement. Degree bi-4 is both necessary and sufficient for flexibility-increasing G^1-refinability within a bi-quadratic C^1 spline complex. Sufficiency is proven by two alternative flexibly G^1-refinable constructions exhibiting good highlight line distributions.

1. Introduction

For a regular quadrilateral mesh, interpreting the nodes as coefficients of uniform tensor-product biquadratic (bi-2) splines offer a simple and low-cost way to obtain a smooth surface. Refining the structure by knot insertion provides new local modelling parameters. Classical generalized subdivision surfaces [1, 2] transfer this advantage to sub-meshes with where $n \neq 4$ quads join or that include n-sided facets. However, subdivision surfaces consist formally of an infinite sequence of contracting surface rings, incompatible with many main-stream computer-aided design (CAD) systems, and accurately computing integral properties near the limit point is costly.

Alternatively an n-sided surface cap can be assembled from a finite number of polynomial pieces, called patches, that are joined with geometric smoothness, i.e. with derivatives matching after reparameterization. This patch-based representation is compatible with CAD systems and allows for immediate engineering analysis [3]. However, minimal degree G^1 constructions that complement bi-2 C^1 splines with bi-3 multi-sided caps, such as [4] abbreviated G_{KP} hereafter, are not refinable in the anticipated way: along certain curves, the refinement does not provide new degrees of freedom, giving the space and shape an unexpected stiffness. This raises the question as to the minimal polynomial degree required for refinement that increases flexibility, i.e. when is a space *flexibly refinable*?

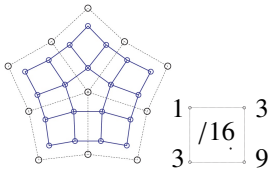

Figure 1: Conversion to a DS-net • via the stencil of *regular* bi-2 spline refinement in the neighborhood of an n-valent vertex.

This paper starts by proving that the degree of flexibly G^1-refinable smooth caps must be at least bi-4. The proof focuses on meshes with n-sided facets, whose 1-neighborhood is abbreviated as DS-nets due to their prominence in Doo-Sabin subdivision [1]. Meshes where $n \neq 4$ quads join in a bi-2 spline complex can be simply converted to DS-nets by applying the well-known formula and stencil for *regular* bi-2 spline knot insertion, see Fig. 1. Since it only transforms Hermite data for filling a hole rather than filling it, this knot insertion does not introduce the shape artifacts commonly observed when applying generalized Doo-Sabin subdivision to n-sided configurations.

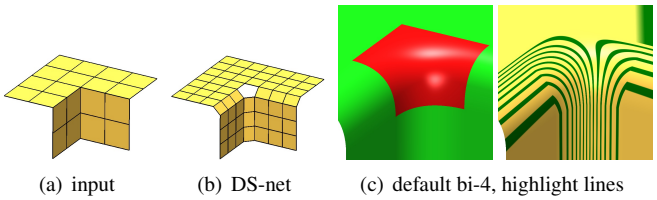

(a) input (b) DS-net (c) default bi-4, highlight lines

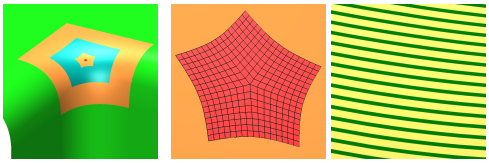

(d) bi-4 alt (e) n 2 × 2 bi-4, highlight lines

Figure 2: Overview of the constructions discussed in this paper for (a) $n = 5$, a two-beam quad net example. (b) DS-net as once refined net. (c) Bi-4 refinable multi-sided surface surrounded by bi-2 surface ring defined by the outer regular input net. (d) Alternative hybrid of *contracting rings and a tiny cap*. (e) BB-net of tiny cap consisting of n bi-4 2 × 2 macro-patches, C^1-connected to surrounding bi-4 ring and its highlight lines.

Conversely, to establish what polynomial degree suffices to

*Corresponding author
Email addresses: kestutis.karciauskas@mif.vu.lt (Kęstutis Karčiauskas), jorg.peters@gmail.com (Jörg Peters)

construct flexibly G^1-refinable multi-sided surfaces with highlight line distributions [5] as good or better than those of the bi-2 tensor-product splines, this paper develops two alternative bi-4 constructions. The first consists of n patches joined with geometric continuity, see Fig. 2c. The second is a hybrid consisting of 3 or 4 guided C^1-joined rings capped by a tiny bi-4 cap that is itself flexibly G^1-refinable (although this is typically not needed, see Fig. 2d,e,f). While more complex, the hybrid construction offers C^1 transitions almost everywhere; that is desirable for downstream use such as texturing or engineering analysis. Moreover geometric modification is simpler and more intuitive than for the first option. That is, the hybrid conveniently supports both adaptive geometry and analysis.

In summary, the contributions of this paper are

- a proof that refinement of reasonable bi-3 G^1 constructions, of multi-sided surface caps in a bi-2 C^1 spline complex, can not increase flexibility along all G-edges;
- a flexibly G^1-refinable bi-4 construction using n pieces per cap and yielding surfaces with good highlight line distributions; and
- an alternative flexibly G^1-refinable hybrid construction of C^1-joined guided rings closed by a tiny cap.

Both constructions are proven to be flexibly G^1-refinable by exhibiting all new degrees of freedom under refinement.

1.1. Related literature

This paper may be viewed as a prequel and complementary to the recent publication [6] that established that flexibly G^2-refinable multi-sided surfaces for inclusion into C^2 bi-cubic splines require degree no less than bi-6; and presented a bi-6 construction. Compared to the present G^1 scenario, the G^2 flexibility bounds, proofs and the corresponding construction of multi-sided surfaces are technically considerably more complicated and so, potentially, obscure some of the underlying principles. The complementary results for flexibly G^1-refinable multi-sided surfaces in this paper not only newly establishes the facts for lower smoothness, but clarifies the arguments and simplifies constructions.

Akin to the new alternative bi-4 subdivision-tiny-cap hybrid of this paper, the construction of [7] provides refinable multi-sided surfaces to cover multi-sided holes in a bi-2 spline complex leveraging several steps of subdivision. However its central cap is not refinable and the overall multi-sided surface has worse shape than the new hybrid. Similarly, the surfaces obtained by smooth multi-sided blending of biquadratic splines in [4] fail to be refinable. The surface caps of [8] are of least degree, but are not refinable and can have poor shape. Filling multi-sided holes in a bi-2 patch complex with S-patches [9] results in high rational degree. The Bi-2 T-splines in [10, 11] do not address multi-sided configurations.

Standard bi-2 subdivision for inclusion into a C^1 spline complex, Doo-Sabin subdivision [1] and Augmented Subdivision [12], not only have the handicap of an infinite sequence of polynomial pieces, but also fail to produce high-end shape (see e.g. [7]; ([12] fails to a much lesser degree).

Overview. Section 2 defines the basic construction tools and defines when constructions are flexibly refinable. Section 3 proves that multi-sided bi-3 G^1 constructions is not flexibly G^1-refinable. Section 4 presents a bi-4 G^1 construction for multi-sided surface regions, suitable for inclusion into a bi-2 C^1 spline complex and Section 5 shows the construction exhibits new degrees of freedom along boundaries and hence is flexibly G^1-refinable. Section 6 presents an alternative flexibly G^1-refinable hybrid construction based on C^1-joined guided rings.

2. Setup and Definitions

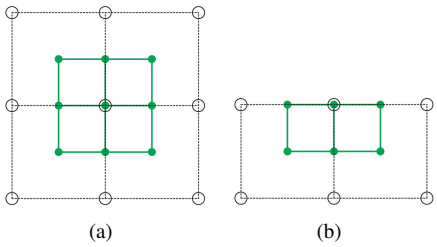

Figure 3: Bi-2 B-to-BB conversion. Solid disks • mark BB-coefficients, circles ∘ mark B-spline control points.

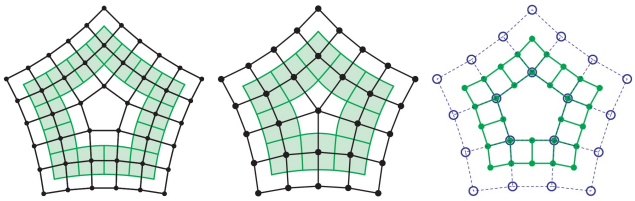

Figure 4: (a) Bi-2 ring from a DS-net. (b) Bi-2 ring from a quad-mesh. Due to knot insertion, to convert to a DS-net, the number of patches quadruples. (c) Tensor-border of degree 2 from a DS-net.

The multi-sided surfaces will be a collection of tensor-product patches of bi-degree d (short bi-d) in Bernstein-Bézier form (BB-form), see e.g. [13]:

$$\mathbf{f}(u,v) := \sum_{k=0}^{d}\sum_{\ell=0}^{d} \mathbf{f}_{k\ell} B_k^d(u) B_\ell^d(v), \quad (u,v) \in [0..1]^2.$$

Here $B_i^d(t) := \binom{d}{i}(1-t)^{d-i}t^i$ are the Bernstein polynomials of degree d and $\mathbf{f}_{ij}$ are the BB-coefficients. We abbreviate $\mathbf{f} := \sum_{k=0}^{d} \mathbf{f}_k B_k^d$ as

$$\mathbf{f} \sim [\mathbf{f}_0, \ldots, \mathbf{f}_d]$$

and define the *layer curves* $\mathbf{f}_j \sim [\mathbf{f}_{0j}, \ldots, \mathbf{f}_{dj}]$. Connecting $\mathbf{f}_{ij}$ to $\mathbf{f}_{i+1,j}$ and $\mathbf{f}_{i,j+1}$ wherever possible yields the *BB-net*. A useful operation on polynomials in BB-form is to split them into two pieces, say a left half and a right half, by the well-known *de Casteljau algorithm* [13].

The vertices of any 3×3 sub-grid in the mesh, such as the grey net in Fig. 3a, can be interpreted as the control net of a uniform bi-2 B-spline [14]. The *B-to-BB conversion* expresses the spline

in bi-2 BB-form illustrated by the green BB-net in Fig. 3a. A partial conversion from a partial mesh yields a sub-net of the BB-net. A sub-net that defines position, and derivatives across an edge is called a *tensor-border*. Fig. 3b shows a first-order tensor-border. Fig. 4a illustrates how B-to-BB conversion creates a surrounding bi-2 surface ring and Fig. 4b shows the same for a quad-mesh with an n-valent vertex. Fig. 4c shows how the partial conversion extends the patch ring of Fig. 4a to a tensor-border.

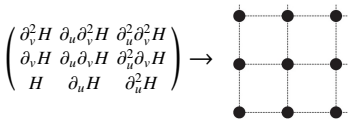

Figure 5: Hermite data as partial derivatives converted to BB-form.

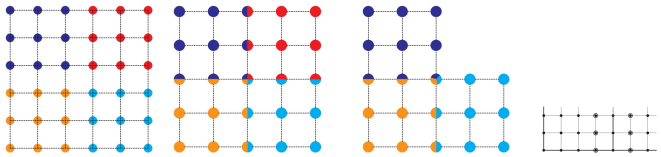

(a) bi-5 (b) bi-4 (c) bi-4 L-shape and C^2 correction

Figure 6: Hermite operators H^k, $k = 5, 4$: (a,b) full patch; (c) L-shaped bi-4 tensor-border and its C^2 correction modifying the circled BB-coefficients.

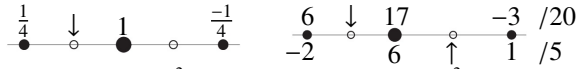

(a) equal degree C^2-join (b) *deg*4-*deg*3 C^2-join

Figure 7: C^2-join at the common (big ●) endpoint. (a) Stencil for the BB-coefficient marked ↓, the unmarked ∘ is defined by symmetry. (b) C^2-join of the curves of *left* - degree 4 and *right* - degree 3.

Jets of derivatives, often sampled from more complex patches and tensor-borders, can be expressed as BB-sub-nets, see Fig. 5. The sub-nets can be assembled into new low degree patches of various degrees Fig. 6a,b (averaging jet-information where it overlaps as in (b)) or parts of tensor-borders, the L-shapes of Fig. 6c. For good shape, it pays to adjust bi-4 L-shapes to join C^2 where they meet along sectors; this is done applying to the circled BB-coefficients the stencil in Fig. 7a.

We will use the functional

$$\mathcal{F}_k f := \int_0^1 \int_0^1 \sum_{i+j=k, i,j\geq 0} \frac{k!}{i!\,j!} (\partial_s^i \partial_t^j f(s,t))^2 \, ds\, dt \qquad (1)$$

to set extra degrees of freedom.

Characteristic parameterizations. The subdominant eigenvalue of subdivision determines the contraction of the subdivision rings towards the limit. The subdominant eigenvalue of bi-3 adjustable speed subdivision [15] with 'speed' parameter $\sigma \in (0..1)$ and $\tilde{\sigma} := 1 - \sigma$ is

$$\lambda_\sigma := \frac{\tilde{\sigma}}{2}((1+\mathsf{c})\sigma^2 + 2\tilde{\sigma} + \sigma\sqrt{(1+\mathsf{c})((1+\mathsf{c})\sigma^2 + 4\tilde{\sigma})}),\ \mathsf{c} := \cos\frac{2\pi}{n}.$$

For $\sigma := \frac{1}{2}$ adjustable speed subdivision coincides with Catmull-Clark subdivision.

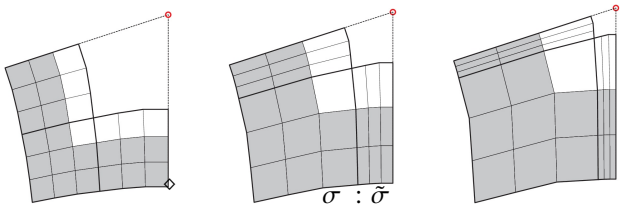

(a) $\sigma := \frac{1}{2}$ (CC) (b) $\sigma := \frac{3}{4}$ (c) $\sigma := \frac{7}{8}$

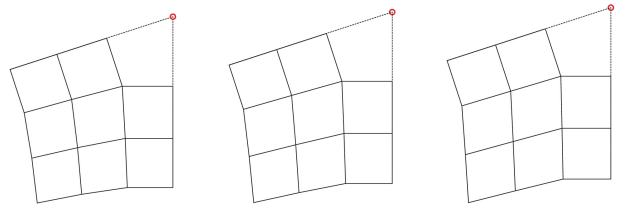

(d) $\sigma := \frac{1}{2}$ (CC) (e) $\sigma := \frac{3}{4}$ (f) $\sigma := \frac{7}{8}$

Figure 8: Maps χ_σ (*top* row) and $\tilde{\chi}_\sigma$ (*bottom* row) for different speeds σ.

Fig. 8,*top* displays characteristic maps χ_σ for one sector and $n = 5$. In the analysis of Catmull-Clark subdivision the maps χ_σ contain the key analytic information. In guided subdivision, however, the corresponding characteristic tensor-borders $\tilde{\chi}_\sigma$ of degree 3 and order 2 (see Fig. 8,*bottom*) are in the forefront. The gray underlaid BB-coefficients of χ_σ are the result of splitting $\tilde{\chi}_\sigma$ in the ratio $\sigma : \tilde{\sigma}$ (see Fig. 8b). We normalize so the corner BB-coefficients (marked as ⋄ in Fig. 8a) are at distance 1 from the center ∘. While different σ result in different χ_σ their tensor-borders $\tilde{\chi}_\sigma$, although slightly different, look alike. This allows a gentle switch to higher speeds, while λ_σ-scalability of characteristic maps and tensor-borders enables an efficient implementation of the sampled guided rings.

Definition 1 (**G^1 constraints**). *Two surface pieces* $\tilde{\mathbf{f}}$ *and* $\mathbf{f}$ *sharing a boundary curve* $\mathbf{e}$ *join* G^1 *if there exists a suitably oriented and non-singular reparameterization* $\rho : \mathbb{R}^2 \to \mathbb{R}^2$ *so that the partial derivatives* $\partial^k \tilde{\mathbf{f}}$ *and* $\partial^k(\mathbf{f} \circ \rho)$, $k = 0, 1$, *agree along* $\mathbf{e}$.

Throughout, we will choose $\mathbf{e}$ to correspond to surface patch parameters $(u, 0 = v)$. Then the relevant Taylor expansion (up to degree 1) of the reparameterization $\mathbb{R}^2 \to \mathbb{R}^2$ with respect to v is

$$\rho(u, v) := (u + b(u)v, a(u)v). \qquad (2)$$

By the chain rule of differentiation, this yields the well-known G^1 constraints in terms of univariate scalar functions $a(u)$, $b(u)$ and the vector-valued functions $\mathbf{f}(u, 0)$, $\tilde{\mathbf{f}}(u, 0)$

$$\partial_v \tilde{\mathbf{f}} = a(u)\, \partial_v \mathbf{f} + b(u)\, \partial_u \mathbf{f}. \qquad (3)$$

Considering n surface sectors surrounding a central point, the sectors are constructed *diagonally symmetric* if the formulas that define $\mathbf{f}_{ji}$ can be obtained from those defining $\mathbf{f}_{ij}$ by exchanging i and j. The construction has *no bias* if the constraints

(3) remain the same when $\tilde{\mathbf{f}}$ and $\mathbf{f}$ are exchanged. No bias implies $a(u) := -1$. Diagonal symmetry and no bias are necessary to preserve input symmetry and generate the same output under re-labeling (re-naming) of mesh vertices.

The purpose of refining a space is typically to gain the additional degrees of freedom for geometric modelling or for engineering analysis.

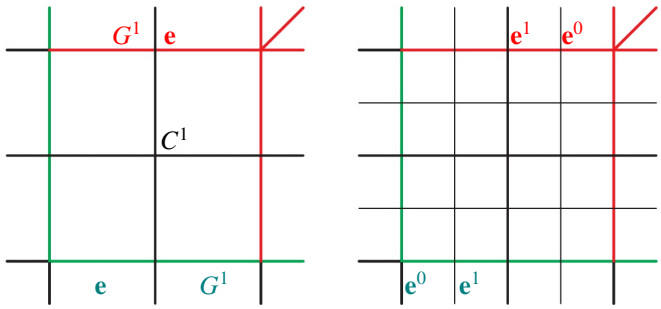

(a) initial (b) refined

Figure 9: G-spline refinement. To be flexibly refinable, new degrees of freedom must appear both in the interior and along the red sector-separating curve boundaries and the green boundaries that connect the cap to the remaining surface.

G-spline spaces and refinement. If we specify a reparameterization $\rho_{\mathbf{e}}$ for every edge $\mathbf{e}$ then a space G_ρ of tensor-product BB-patches joined with the same reparameterizations forms a linear vector space. That is, any linear combination of elements in G_ρ is again in G_ρ.

The space G_ρ is *refinable* to a space $\dot{G}_{\dot\rho}$ in the following sense, see Fig. 9. For each polynomial piece $\mathbf{f} \in G_\rho$ defined on $\square := [0..1]^2$, the space $\dot{G}_{\dot\rho}$ has four polynomial pieces $\mathbf{f}^r$, $r = 1, 2, 3, 4$ (wlog. of the same degree as $\mathbf{f}$) defined on the four quarters of $\square$ and joined by the following reparameterizations $\dot\rho$: the Taylor expansion $\dot\rho$ up to degree 1 across the new four inner edges $\dot\rho$ is the identity, i.e. the pieces join C^1; along any original edge $\mathbf{e}$ the ρ is retained in pieces:

$$\rho_{\mathbf{e}^0}(u,v) = \rho_{\mathbf{e}}(\frac{u}{2}, \frac{v}{2}), \quad \rho_{\mathbf{e}^1}(u,v) = \rho_{\mathbf{e}}(\frac{1}{2} + \frac{u}{2}, \frac{v}{2}).$$

Then there is a choice of $\mathbf{f}^r$, namely applying de Casteljau's algorithm to $\mathbf{f}$ at $u = v = 1/2$, so that any element $\mathbf{f} \in G_\rho$ can be represented in $\dot{G}_{\dot\rho}$. That is, $\dot{G}_{\dot\rho}$ refines G_ρ. Since many other choices of macro-patches $\mathbf{f}^r$ are allowable, the $\dot{G}_{\dot\rho}$ can be expected to provide more flexibility than G_ρ, i.e. has more degrees of freedom, e.g. BB-coefficients not constrained by enforcing smoothness.

In the next section, we will see that refined functions can remain a single polynomial along the reparameterized G-edges. This failure of the expected additional degrees of freedom to materialize under refinement is shown to preclude the use of bicubic multi-sided surfaces for applications requiring increasing freedom and motivates the following definition.

Definition 2 (flexibly refinable). *With the preceding definition of $\dot{G}_{\dot\rho} \subsetneq G_\rho$ a construction is flexibly refinable if, for each domain piece $\square$, $\dot{G}_{\dot\rho}$ has more degrees of freedom than G_ρ, both along map boundaries and in the interior.*

In [16] the term 'locking' was used to describe a similar lack of increase in flexibility. Due to the established use of the term locking for a different concept in engineering shell analysis we prefer flexibility-increasing, or short, flexible refinement.

Definition 2 represents a compromise between the intuitive characterization for practical piecewise polynomial constructions and a more abstract characterization of a universal nature. In the regular case of tensor-product B-splines practical and abstract are elegantly combined via knot insertion – but in the multi-sided setup, parameterization changes across G-curves and knots can only be inserted in separate 'sectors'.

The counting of degrees of freedom as unconstrained B- or BB-coefficients (or both) is a classical approach of geometric design [17, 18, 19] to establish the dimension of a piecewise polynomial spline space. Since the dimension does not depend on the choice of basis degrees of freedom can be redistributed. We will see that, fortuitously, for G^1-continuity many unconstrained BB-coefficients naturally reside on the sector-separating curve.

In this paper, we focus on multi-sided caps whose sectors are internally C^1. That is the black transitions in Fig. 9 are C^1. In the context of refinement it is natural to focus on internally C^1 sectors since all new internal transitions arising from refinement must be parametrically C^1 to reproduce the original polynomial pieces by the finer construction. Moreover, constructions with internally G^1 sectors are not only more complicated, but, in our experience, yield lower surface quality.

3. Bi-3 G^1 constructions are not flexibly refinable

This section proves that G^1 constructions for multi-sided caps surrounded by C^1 bi-2 spline surfaces must have degree at least bi-4 if they are to be flexibly G^1-refinable and satisfy the canonical requirement of spline surface construction: no bias and diagonally symmetric internally C^1 sectors. The proof consists of multiple lemmas.

First we note that only polynomial reparameterizations need to be considered.

Proposition 1. *For an unbiased G^1 construction,*

(i) the functions a, b of the reparameterization ρ across $\mathbb{c}^s$,$\mathbb{m}^s$ must be polynomials;
(ii) across $\mathbb{m}^s$,$\mathbb{o}$, $a \equiv -1$ and b must be a polynomial.

The proof of Proposition 1 is in the Appendix.

Connecting the sectors of a finite multi-sided G^1 construction typically requires *reparameterization along the input boundary* $\mathbb{c}^s$, $\mathbb{m}^s$ in order to smoothly join with the surrounding surface. Fig. 10b depicts a uniform split of tensor-border $\mathbf{t}$ of one sector into pieces $\mathbf{t}^k$, $k = 0, 1, \ldots, N$. Each piece is reparameterized by a local map $\rho^k : [0..1] \to \rho^k(u,v) := (u + b^k(u)v, a^k(u)v)$ defined in terms of local a^k, b^k (see (2)) to yield new tensor-borders $\tilde{\mathbf{t}}^k$.

In the following we denote as $\deg h$ the degree of function h in u-direction.

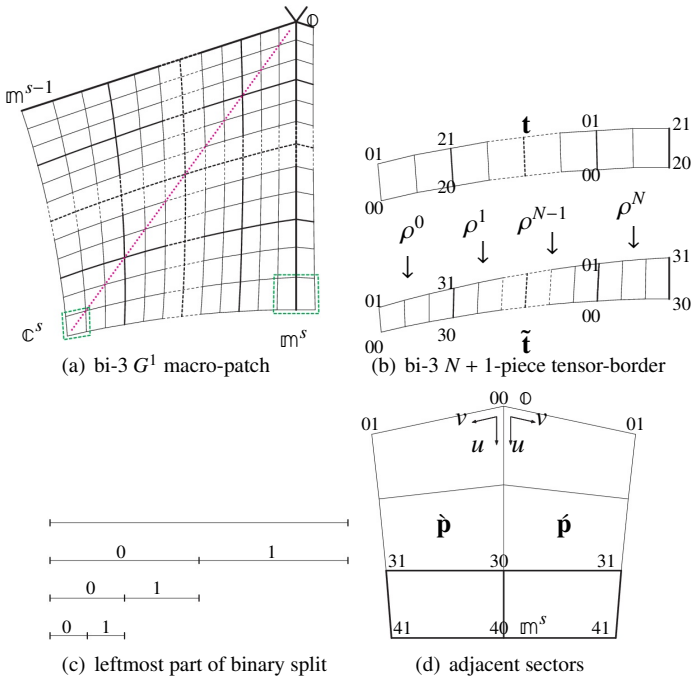

(a) bi-3 G^1 macro-patch (b) bi-3 $N+1$-piece tensor-border

(c) leftmost part of binary split (d) adjacent sectors

Figure 10: Hypothetical bi-3 G^1-refinable multi-piece (macro-patch) construction. (a) Layout of internally C^1 macro-patch. (b) Reparameterization of the $N+1$-piece C^1 input tensor-border $\mathbf{t}$ yields $\tilde{\mathbf{t}}$. (c) *From top*: row 1 – initial piece $\mathbf{t}^k$; row 2 – first split; rows 3,4 – left parts of consecutive splits. (d) G^1-join of neighbor sectors sharing the tensor-border.

Lemma 1. *(***degree bounds of ρ across $\mathbb{c}^s$,$\mathbb{m}^s$***). If the tensor-borders* $\mathbf{t}$ *are of degree bi-2 and the reparameterized tensor-borders are of degree bi-3 then* $\deg a^k \le 1$ *and* $\deg b^k \le 2$.

Proof Counting confirms that the stated choice of degrees yields tensor-borders $\tilde{\mathbf{t}}^s$ of degree 3 in u-direction. To show that the listed degrees are maximal, replace in (3) $\mathbf{f}$ by $\mathbf{t}^k$ and $\tilde{\mathbf{f}}$ by $\tilde{\mathbf{t}}^k$ to see $3 = \deg \tilde{\mathbf{t}}^k = \max\{\deg a^k + \deg \mathbf{t}^k, \deg b^k + \deg \mathbf{t}^k - 1\} = \max\{\deg a^k + 2, \deg b^k + 1\}$. Then $\deg a^k \le 1$ and $\deg b^k \le 2$. |||

Next, we show that either $b_0^k + 2b_1^k + b_2^k = 0$ or the boundary remains a single quadratic curve under refinement.

Lemma 2. *The bi-3 tensor-border* $\tilde{\mathbf{t}}^k$ *is binary flexibly G^1-refinable only if* $b_0^k + 2b_1^k + b_2^k = 0$.

Proof Binary splitting of the tensor-borders $\mathbf{t}^k$, $\tilde{\mathbf{t}}^k$ (see Fig. 10c) into $\mathbf{t}^{k,i}$, $\tilde{\mathbf{t}}^{k,i}$, $i \in \{0,1\}$ and preserving geometric smoothness implies reparameterizations $\rho^{k,r}$, $r = 0, 1$ with

$$\begin{aligned} a^{k,0}(u) &:= a^k(\frac{u}{2}),\ a^{k,1}(u) := a^k(\frac{1}{2} + \frac{u}{2}), \\ b^{k,0}(u) &:= b^k(\frac{u}{2}),\ b^{k,1}(u) := b^k(\frac{1}{2} + \frac{u}{2}). \end{aligned} \tag{4}$$

Since consecutive pieces $\mathbf{t}^{k,0}$ and $\mathbf{t}^{k,1}$ are assumed to be C^1-connected, see Section 2 on G^1 refinement, along the boundary curve also $\tilde{\mathbf{t}}^{k,0}$ and $\tilde{\mathbf{t}}^{k,1}$ must be C^1-connected. Setting equal the expansions of the first derivative of the reparameterized boundary $\tilde{\mathbf{t}}^{k,0}$ and $\tilde{\mathbf{t}}^{k,1}$ and

$$\partial_u \tilde{\mathbf{t}}^{k,i} = \partial_u a^{k,i} \partial_v \mathbf{t}^{k,i} + a^{k,i} \partial_{vu} \mathbf{t}^{k,i} + \partial_u b^{k,i} \partial_u \mathbf{t}^{k,i} + b^{k,i} \partial_{uu} \mathbf{t}^{k,i},$$

when equating $(\partial_u \tilde{\mathbf{t}}^{k,0})(1) = (\partial_u \tilde{\mathbf{t}}^{k,1})(0)$, we observe that (due to C^1 continuity of the $a^{k,i}$, $b^{k,i}$ and $\mathbf{t}^{k,i}$) three of the four terms agree and only

$$b^{k,0}(1)\partial_{uu}\mathbf{t}^{k,0}(1) = b^{k,1}(0)\partial_{uu}\mathbf{t}^{k,1}(0) \tag{5}$$

has to hold. (5) holds if and only if the boundary curves $\mathbf{t}^{k,0}(u,0)$ and $\mathbf{t}^{k,1}(u,0)$ are C^2-connected – or $b^{k,0}(1) = b^{k,1}(0) = b_0^k + 2b_1^k + b_2^k = 0$. The claim follows since the first option means that the boundary remains a single quadratic curve under refinement, i.e. the refinement does not increase flexibility. |||

Lemma 3. *The bi-3 tensor-border* $\tilde{\mathbf{t}}^k$ *is binary flexibly G^1-refinable only if* $b^k(u) \equiv 0$ *for all* $k = 0, \dots, N$. *Diagonal symmetry additionally implies all* $a^k(u) \equiv 1$.

Proof We focus on the left pieces (see Fig. 10c) of an iterated binary split. The C^1 connectedness of consecutive pieces $\mathbf{t}^{k,0}$ and $\mathbf{t}^{k,1}$ and Lemma 2 imply that $b_2^k := -b_0^k - 2b_1^k$. Repeating the splitting of the simplified $b^{k,0} \sim [b_0^k, \frac{b_0^k}{2} + \frac{b_1^k}{2}, 0]$, and applying Lemma 2 again yields $3b_0^k + b_1^k = 0$ and hence for the left part $\sim [b_0^k, -\frac{b_0^k}{4}, 0]$. Another repeat yields $b_0^k := 0$, i.e. $b^k(u) \equiv 0$. Considering the part of $\tilde{\mathbf{t}}^0$ marked by the left □ in Fig. 10a, diagonal symmetry implies $a^0(u) \equiv 1$. Since we assume that the sectors are internally C^1, $\tilde{t}^k$ and $\tilde{t}^{k+1}$ are C^1-connected. Therefore equality holds for $(\partial_v \tilde{t}^k)(1) = (\partial_v \tilde{t}^{k+1})(0)$ and its first derivative in the u-direction. Together with $b^i(u) = 0$ this implies that a^k and a^{k+1} join C^1. Since all a^i are linear they must equal 1. |||

Lemma 3 implies that $\tilde{\mathbf{t}}^k$ is $\mathbf{t}^k$ in degree-raised form. Therefore the first-order expansions of adjacent sectors at $\mathbb{m}$ (represented by 2×2 BB-coefficients each) join C^1: $\acute{\mathbf{p}}_{i1} := 2\acute{\mathbf{p}}_{i0} - \acute{\mathbf{p}}_{i1}$, $i = 2, 3$. To prove the main theorem of this section now only requires analyzing the refinement along the sector-separating curves.

Theorem 1. *Symmetric, unbiased, multi-sided bi-3 G^1 surfaces with internally C^1 sectors that are suitable for inclusion into C^1 bi-2 splines are not flexibly G^1-refinable.*

Proof Neighboring polynomial pieces $\grave{\mathbf{p}}$, $\acute{\mathbf{p}}$ of degree bi-3 join without bias the tensor-borders $\grave{\mathbf{t}}^N$, $\acute{\mathbf{t}}^0$ (see the right □ in Fig. 10a and the indices in Fig. 10d) with constraints $\partial_v \acute{\mathbf{p}} = -\partial_v \grave{\mathbf{p}} + b(u)\partial_u \grave{\mathbf{p}}$ (3). Since $\acute{\mathbf{p}}_{i1} := 2\grave{\mathbf{p}}_{i0} - \grave{\mathbf{p}}_{i1}$, $i = 2, 3$, the least degree $b(u) \neq 0$ is $b(u) := \gamma(1-u)^2$ for some constant γ. Comparison of degrees then implies that the actual degree of the sector-separating curve is at most 2.

Similarly as in Lemma 2, one refinement step implies that the sector-separating curve must be C^2-connected and without increased flexibility, or $\gamma = 0$ and hence $\acute{\mathbf{p}}_{i1} := 2\grave{\mathbf{p}}_{i0} - \grave{\mathbf{p}}_{i1}$, for all $i = 0, 1, 2, 3$. But the latter means that no progress is made to meet the constraints of the n-sided configuration at $\mathbb{o}$, and further partitioning is useless. |||

4. A geometric bi-4 construction

This section defines a flexibly G^1-refinable, diagonally symmetric, unbiased, multi-sided G^1 bi-4 construction suitable for

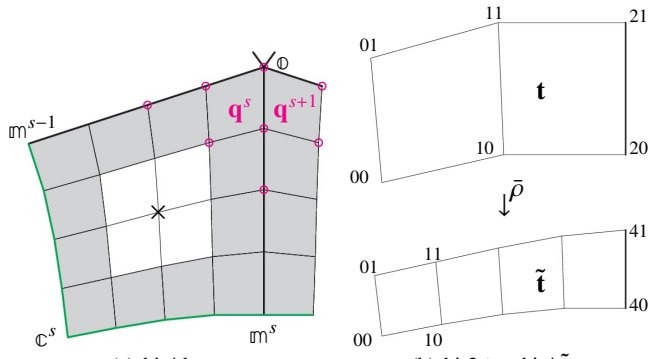

(a) bi-4 layout (b) bi-2 $\mathbf{t} \to$ bi-4 $\tilde{\mathbf{t}}$

Figure 11: (a) Layout of bi-4 G^1 cap. (b) Reparameterization $\bar\rho$ of input bi-2 tensor-border $\mathbf{t}$ to $\tilde{\mathbf{t}}$.

inclusion into bi-2 C^1 spline complex. While imposing formal smoothness is easy, achieving good surface quality requires additional effort such as enforcing well-defined curvature at the extraordinary point. Another key is to carefully merge the G^1-join via ρ between sectors and the G^1-join via the reparameterization $\bar\rho$, defined as in (2), to the input bi-2 data by combining the re-parameterizations as a map τ.

Fig. 11a shows the layout of the new construction. Each of n sectors is a single bi-4 polynomial patch. The BB-coefficients marked as $\circ$ represent Hermite data up to order 2 at the extraordinary point; that is they represent the *quadratic expansion* $\mathbf{q}$ obtained from a map $\tilde{\mathbf{q}}$ of total degree 2 reparameterized by τ. Between sectors (along $\mathbb{o}$, $\mathbb{m}^s$) and along the green boundary to the input data ($\mathbb{m}^{s-1}$, $\mathbb{c}^s$, $\mathbb{m}^s$) G^1-continuity is enforced by the choice of the BB-coefficients delineating the gray strips.

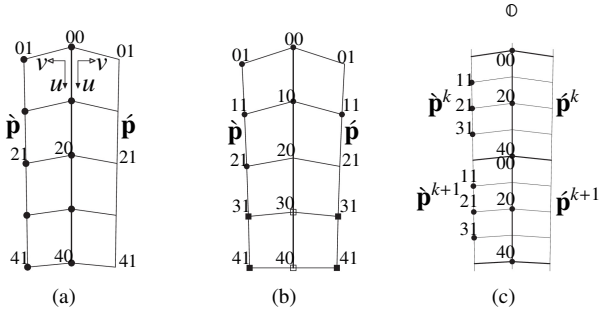

Figure 12: G^1 constraints between sectors along sector-separating curve from $\mathbb{o}$ to $\mathbb{m}$. (a) Generic piece. (b) Initial piece with 00 corresponding to $\mathbb{o}$ and 40 corresponding to $\mathbb{m}$. (c) Generic pieces k and $k+1$ during refinement.

Fig. 12a shows a generic refined piece along a sector-separating curve constrained by

$$\partial_v \acute{\mathbf{p}} = -\partial_v \grave{\mathbf{p}} + b(u)\partial_u \grave{\mathbf{p}}, \quad b(u) := b_0(1-u) + b_1 u.$$

A solution, whose unconstrained BB-coefficients are marked as $\bullet$ in Fig. 12a, has the form

$$\acute{\mathbf{p}}_{i1} := 2\grave{\mathbf{p}}_{i0} - \grave{\mathbf{p}}_{i1} + \frac{1}{4}\mathbf{f}_i, i = 0,\dots,4, \ [\mathbf{f}_0,\dots,\mathbf{f}_4] \sim b(u)\partial_u \grave{\mathbf{p}}. \quad (6)$$

For initial cap in Fig. 11a we take $b(u) := 2\mathsf{c}(1-u)$ and re-arrange the solution (6) into the form

$$\begin{aligned}
\acute{\mathbf{p}}_{i0} &:= \grave{\mathbf{p}}_{i0}, i = 0,\dots,4, \\
\acute{\mathbf{p}}_{01} &:= -\grave{\mathbf{p}}_{01} + 2\mathsf{c}\grave{\mathbf{p}}_{10} + 2(1-\mathsf{c})\grave{\mathbf{p}}_{00}, \qquad (7)\\
\grave{\mathbf{p}}_{20} &:= \frac{(3\mathsf{c}-4)\grave{\mathbf{p}}_{10} + 2(\grave{\mathbf{p}}_{11} + \acute{\mathbf{p}}_{11})}{3\mathsf{c}}, \qquad (8)\\
\acute{\mathbf{p}}_{21} &:= -\grave{\mathbf{p}}_{21} + (2-\mathsf{c})\grave{\mathbf{p}}_{20} + \mathsf{c}\grave{\mathbf{p}}_{30}, \\
\grave{\mathbf{p}}_{30} &:= \frac{2(\grave{\mathbf{p}}_{31} + \acute{\mathbf{p}}_{31}) - \mathsf{c}\grave{\mathbf{p}}_{40}}{4-\mathsf{c}}, \quad \grave{\mathbf{p}}_{40} := \frac{\grave{\mathbf{p}}_{41} + \acute{\mathbf{p}}_{41}}{2}. \qquad (9)
\end{aligned}$$

The assignment of $\acute{\mathbf{p}}_{01}$ enforces tangent plane continuity at the extraordinary point; the relation that determines $\grave{\mathbf{p}}_{30}$ triggers the reparameterization $\bar\rho := [u, a(u)v]$, $a(u) \sim [1, 1, 2/(2-c)]$, of the input tensor-border $\mathbf{t}$, see Fig. 11b. Among the possible choices for $b(u)$, the $b(u) = 0$ is not only the simplest option but also yields the best shape.

The unconstrained middle BB-coefficient $\mathbf{p}_{22}$, marked as $\times$ in Fig. 11a, is defined as in [4], i.e.

$$\begin{aligned}
\mathbf{p}_{22} := &\frac{1}{2}\left(\frac{2}{3}(\mathbf{p}_{21} + \mathbf{p}_{23}) - \frac{1}{6}(\mathbf{p}_{20} + \mathbf{p}_{24})\right) + \\
&\frac{1}{2}\left(\frac{2}{3}(\mathbf{p}_{12} + \mathbf{p}_{32}) - \frac{1}{6}(\mathbf{p}_{02} + \mathbf{p}_{42})\right).
\end{aligned} \quad (10)$$

Here the pattern $\frac{2}{3}(\mathbf{p}_1 + \mathbf{p}_3) - \frac{1}{6}(\mathbf{p}_0 + \mathbf{p}_4)$ indicates reduction to degree 3. Reducing the degree is a heuristic that reduces the number of free parameters and so impedes high-frequency fluctuations of the surface.

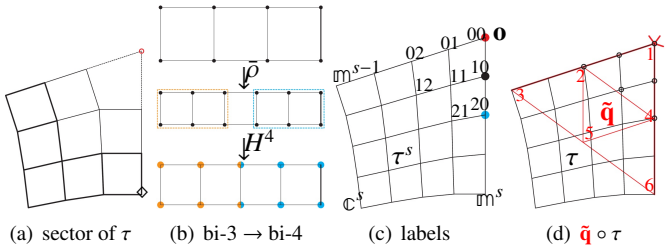

(a) sector of τ (b) bi-3 $\to$ bi-4 (c) labels (d) $\tilde{\mathbf{q}} \circ \tau$

Figure 13: Reparameterization τ. (a) Marked by thick lines are the first-order Hermite data (tensor-border) of the characteristic map [2] (Catmull-Clark subdivision). The map is normalized so that a distance between $\diamond$ and $\circ$ equals 1. (b) Transformation $H^4 \circ \bar\rho$. (c) Setting $\bullet := \frac{1}{2}\bullet + \frac{1}{2}\bullet$ (for all valencies n) improves the distribution of the BB-coefficients of τ and simplifies the technical formulas. (d) When sampling $\tilde{\mathbf{q}} \circ \tau$, only the circled BB-coefficients, τ_{ij}, $i + j \le 2$, of $\tilde{\mathbf{q}}$ are involved.

4.1. *Parameterization τ and quadratic expansion* $\mathbf{q}$

The map τ is a planar, rotationally-symmetric version of the general bi-4 construction: the transformation $H^4 \circ \bar\rho$ (see Fig. 13b) is applied to the first-order Hermite data (in Fig. 13a indicated by thick lines) of the tensor-border of the characteristic map of Catmull-Clark subdivision (shown in Fig. 8). Due to normalization of characteristic map, the points $\mathbb{m}^s$ are the vertices of a regular unit n-gon with center $\mathbb{o} = \mathbf{o}$. The BB-coefficients of τ satisfy (7), (8), (9) and (10). The free parameters of this setup allow to set $\bullet := \frac{1}{2}\bullet + \frac{1}{2}\bullet$, see Fig. 13b. Due to rotational and diagonal symmetry of τ, there are only two free

parameters remaining and they are set to minimize the functional $\mathcal{F}_4$, see (1), over one sector. In summary, with the labels in Fig. 13b, and unlisted BB-coefficients obtained by symmetry, $\bar\rho$ and formula (10),

$$\tau_{00} := \mathbf{o}, \qquad \kappa := \frac{4+3\mathsf{c}}{8(1+\mathsf{c})}$$

$$\tau_{10} := \frac{1}{2}(\tau_{00}+\tau_{02}),\ \tau_{11} := \kappa(\tau_{20}+\tau_{02}) + (1-2\kappa)\tau_{00},$$

$$\tau_{21} := \mu\tau_{20} + \bar\mu\tau_{02} + (1-\mu-\bar\mu)\tau_{00},\ \tau_{20} := (1-\nu)\mathbb{o} + \nu\mathbb{m}^s.$$

The parameters μ_n, $\bar\mu_n$ and ν_n are (5-digits surfice)
$\mu_3 := 1.218$, $\bar\mu_3 := 0.69516$, $\nu_3 := 0.48921$;
for $n > 4$
$\mu_n := 0.99816 - 0.23281\mathsf{c} + 0.13699\mathsf{c}^2 - 0.04629\mathsf{c}^3$,
$\bar\mu_n := 0.49489 - 0.16062\mathsf{c} + 0.08887\mathsf{c}^2 + 0.01305\mathsf{c}^3$,
$\nu_n := 0.50233 - 0.02008\mathsf{c} - 0.00511\mathsf{c}^2 - 0.03876\mathsf{c}^3$.

Let $\tilde{\mathbf{q}}$ be a map of total degree 2 defined on a regular unit n-gon with a center $\mathbb{o}$ and BB-coefficient labels displayed in Fig. 13d. The following lemma is checked by inspection.

Lemma 4. (quadratic expansion q at $\mathbb{o}$). *For $i+j \le 2$, denote as $\mathbf{q}^s_{ij}$, $\mathbf{q}^{s+1}_{ij}$ the BB-coefficients obtained from converting the partial derivatives of $\mathbf{h} := \tilde{\mathbf{q}} \circ \tau$ up to order 2 to bi-4 BB-form:*

$$\begin{pmatrix} \partial_v^2\mathbf{h} & \partial_v\mathbf{h} & \mathbf{h} \\ \cdot & \partial_u\partial_v\mathbf{h} & \partial_u\mathbf{h} \\ \cdot & \cdot & \partial_u^2\mathbf{h} \end{pmatrix} \to \begin{pmatrix} \mathbf{q}^s_{02} & \mathbf{q}^s_{01} & \mathbf{q}^s_{00} \\ \cdot & \mathbf{q}^s_{11} & \mathbf{q}^s_{10} \\ \cdot & \cdot & \mathbf{q}^s_{20} \end{pmatrix},\ \mathbf{q}^{s+1}_{0i} = \mathbf{q}^s_{i0},\ i = 0,\dots,2. \quad (11)$$

Then the quadratic expansions $\mathbf{q}^s$ and $\mathbf{q}^{s+1}$ join G^1.

Explicitly, by symbolic calculation, $\mathbf{q}^s$ is obtained from the quadratic map $\tilde{\mathbf{q}}^s$ as

$$\begin{pmatrix} \mathbf{q}^s_{00} \\ \mathbf{q}^s_{01} \\ \mathbf{q}^s_{02} \\ \mathbf{q}^s_{10} \\ \mathbf{q}^s_{11} \\ \mathbf{q}^s_{20} \end{pmatrix} := \begin{pmatrix} 1 & 0 & 0 & 0 & 0 & 0 \\ 1-\kappa & \kappa & 0 & 0 & 0 & 0 \\ 1-2\kappa+\frac{2\kappa^2}{3} & \frac{2\kappa(3-2\kappa)}{3} & \frac{2\kappa^2}{3} & 0 & 0 & 0 \\ 1-\kappa & 0 & 0 & \kappa & 0 & 0 \\ 1-4\kappa\nu+\frac{\kappa^2}{2} & \frac{\kappa(4\nu-\kappa)}{2} & 0 & \frac{\kappa(4\nu-\kappa)}{2} & \frac{\kappa^2}{2} & 0 \\ 1-2\kappa+\frac{2\kappa^2}{3} & 0 & 0 & \frac{2\kappa(3-2\kappa)}{3} & 0 & \frac{2\kappa^2}{3} \end{pmatrix} \begin{pmatrix} \tilde{\mathbf{q}}^s_1 \\ \tilde{\mathbf{q}}^s_2 \\ \tilde{\mathbf{q}}^s_3 \\ \tilde{\mathbf{q}}^s_4 \\ \tilde{\mathbf{q}}^s_5 \\ \tilde{\mathbf{q}}^s_6 \end{pmatrix}, \quad (12)$$

where $\kappa := (4+3\mathsf{c})/(8(1+\mathsf{c}))$ and the BB-coefficients of each sector of the quadratic map $\tilde{\mathbf{q}}$ can be defined iteratively via C^2-constraints from an initial sector $\tilde{\mathbf{q}}^0_i, i = 1,\dots,6$.

4.2. The Algorithm

With the indexing of Fig. 13b,

$$S := \{\tilde{\mathbf{q}}^0_i, i = 1,\dots,6;\quad \mathbf{p}^s_{21}, s = 0,\dots,n-1\},$$

the BB-coefficients of patch $\mathbf{p}^s$ are set as follows (cf. Fig. 11a).

(i) $\circ$ by formula (12);
(ii) $\mathbf{p}^{s+1}_{12}$ by formulas (8), (9);
(iii) $\bar\rho$-reparameterized input bi-2 tensor-borders;
(iv) $\times$ by (10);
(v) the $6+n$ BB-coefficients in S by minimizing the functional $\mathcal{F}_3$, see (1), over all n bi-4 patches $\mathbf{p}^s$.

Since the overall construction is linear, it can be executed as a matrix multiplication.

5. G^1-refinability of the bi-4 cap

In this section, we exhibit the unconstrained BB-coefficients of a binarily refined representation.

The refinement amounts to uniform knot insertion for tensor-product bi-4 C^1 splines in the interior of each sector. In Fig. 14, the new unconstrained BB-coefficients are marked as $\bullet$.

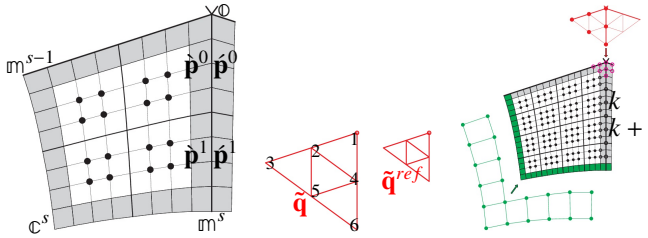

Figure 14: (a) Bi-4 G^1 surface once-refined: new inner degrees of freedom are marked $\bullet$. (b) Refinement of the quadratic map $\tilde{\mathbf{q}}$. (c) The control point groups of the refined bi-4 G^1 surface.

Along $\mathbb{o}$, $\mathbb{m}$, the maps $b^k(u)$ of ρ^k are split into

$$b^{ref,0}(u) := b^k(\frac{u}{2}), \quad b^{ref,1}(u) := b^k(\frac{1}{2}+\frac{u}{2})$$

and then re-label

$$b^{2k}(u) := b^{ref,0}(u),\ b^{2k+1}(u) := b^{ref,1}(u).$$

Along $\mathbb{c}$, $\mathbb{m}$, the analogous split and re-labelling is applied to $a^k(u)$ of $\bar\rho^k$. Then at $\mathbb{m}$, where the refinements along $\mathbb{c}$, $\mathbb{m}$ and $\mathbb{o}$, $\mathbb{m}$ overlap, the 2×2 jets of BB-coefficients agree. Consider Fig. 14c. Along $\mathbb{c}$ $\mathbb{m}$, uniform knot insertion refines the green control points of the C^1 bi-2 spline complex; and B-to-BB conversion followed by reparameterizations $\bar\rho^k$ generates the green-underlaid BB-coefficients of the bi-4 sector. Along the sector-separating curves, using (6) for adjacent pieces ρ^k, ρ^{k+1}, the following lemma is checked by inspection.

Lemma 5. *For $i = 0,\dots,4$, the layer curves $\acute{\mathbf{p}}^k_{i1}$ and $\acute{\mathbf{p}}^{k+1}_{i1}$ are C^1-connected if the layer curves $\grave{\mathbf{p}}^k_{i0}$ and $\grave{\mathbf{p}}^{k+1}_{i0}$ are C^2-connected and $\grave{\mathbf{p}}^k_{i1}$ and $\grave{\mathbf{p}}^{k+1}_{i1}$ are C^1-connected.*

The new unconstrained BB-coefficients are marked as $\bullet$ in Fig. 12c.

5.1. Refinement of quadratic expansion

Defining the quadratic expansion $\mathbf{q}$ by the quadratic map $\tilde{\mathbf{q}}$ and the reparameterization τ, a uniform split (knot insertion) of the bi-4 cap results in $\mathbf{q}^{ref} := \tilde{\mathbf{q}} \circ \tau(\frac{u}{2}, \frac{v}{2})$. Setting $\tilde{\mathbf{q}}^{ref} := \tilde{\mathbf{q}}(\frac{u}{2}, \frac{v}{2})$ (see Fig. 14b), we observe that

$$\begin{pmatrix} \tilde{\mathbf{q}}^{ref}_1 \\ \tilde{\mathbf{q}}^{ref}_2 \\ \tilde{\mathbf{q}}^{ref}_3 \\ \tilde{\mathbf{q}}^{ref}_4 \\ \tilde{\mathbf{q}}^{ref}_5 \\ \tilde{\mathbf{q}}^{ref}_6 \end{pmatrix} := \frac{1}{4}\begin{pmatrix} 4&0&0&0&0&0 \\ 2&2&0&0&0&0 \\ 1&2&1&0&0&0 \\ 2&0&0&2&0&0 \\ 1&1&0&1&1&0 \\ 1&0&0&2&0&1 \end{pmatrix}\begin{pmatrix} \tilde{\mathbf{q}}_1 \\ \tilde{\mathbf{q}}_2 \\ \tilde{\mathbf{q}}_3 \\ \tilde{\mathbf{q}}_4 \\ \tilde{\mathbf{q}}_5 \\ \tilde{\mathbf{q}}_6 \end{pmatrix} \quad (13)$$

Setting $\kappa^{ref} := \frac{1}{4} + \frac{\kappa}{2}$, we calculate $\mathbf{q}^{ref}$ according to (12), with $\tilde{\mathbf{q}}$ replaced by $\tilde{\mathbf{q}}^{ref}$ and κ by κ^{ref}.

5.2. *Linearly independent basis functions*

Considering one coordinate and setting the unconstrained control point values to zero, except for the control point with index α to 1 and then applying the bi-4 cap construction yields a collection of piecewise polynomial functions denoted g^α. The g^α form four separate groups, see Fig. 14c.

(a) Control points • of the surrounding bi-2 splines;
(b) internal C^1-spline coefficients •;
(c) six control points • of the quadratic map $\tilde{\mathbf{q}}$ at $\mathbb{o}$;
(d) the subset of unconstrained BB-coefficients ∘ in the gray G^1-strip that are neither defined by (a) nor (c).

Theorem 2. *The functions g^α are linearly independent.*

Proof Assume that a linear combination $\sum_\alpha x_\alpha g^\alpha$ of functions g^α from all four groups is the zero function, i.e. all BB-coefficients of the resulting cap are zero. We show that then all x_α must be zero.

- The green BB-coefficients of bi-4 cap are obtained by B-to-BB conversion followed by reparameterizations $\bar{\rho}^k$. The control points of B-splines are linearly independent, and none of green BB-coefficients are set by groups (b), (c), (d). Therefore the $x_\alpha = 0$ for α in group (a).
- None of BB-coefficients • in group (b) are set by groups (a), (c), (d). Hence $x_\alpha = 0$ for α in group (b).
- The derivatives up to order 2, evaluated at the $\mathbb{o}$-corner of bi-4 patch, vanish if and only if the 6 control points ∘ of $\mathbf{q}^s$ vanish, i.e. $x_\alpha = 0$ for α in group (c).
- Since the α within group (d) were chosen so that the associated g^α are linearly independent, all $x_\alpha = 0$.

|||

Since the construction is flexibly G^1-refinable the surfaces are also 'analysis-suitable' in the sense of [16]. As later examples will demonstrate, the resulting surfaces are also 'geometry-suitable' in the sense that the highlight line distribution is on par or better than that of the underlying C^1 bi-2 splines. However the new degrees of freedom are not directly suited for geometric manipulations such as adding the detail by local modifications along or across sector separating curve.

6. An alternative guided flexibly G^1-refinable construction

With a focus on local geometric manipulation akin to subdivision surfaces, this section shows how the G^1 bi-4 cap can define a C^1 map of total degree 5 that in turn can guide a sequence of contracting bi-4 surface rings. A tiny cap of the same degree make the construction finite. This yields surfaces that offer uniform parameters for both engineering analysis and for adding geometric detail.

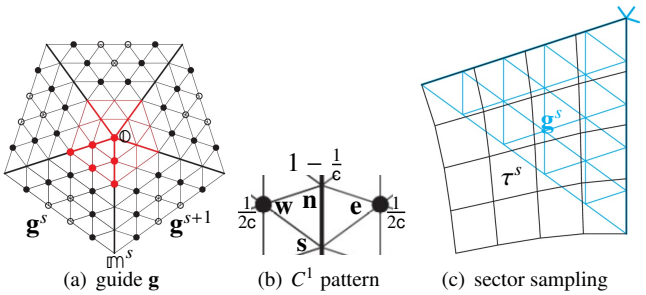

(a) guide $\mathbf{g}$ (b) C^1 pattern (c) sector sampling

Figure 15: (a) C^1 guide of total degree 5. The red part represents a quadratic map $\tilde{\mathbf{q}}$ in degree raised form. (b) C^1 join between sectors enforces a pattern of constraints on the coefficients. (c) Sampling the guide $\mathbf{g}$ with parameterization τ.

6.1. *A C^1 guide of total degree 5*

Fig. 15a shows the structure of C^1 map $\mathbf{g}$ of total degree 5 with a central red quadratic map $\tilde{\mathbf{q}}$ (in degree-raised form) defined by six BB-coefficients • of one sector. To enforce a C^1-join across sector-separating curve, starting with $\mathbf{n}$ as outermost red BB-coefficient, the relation illustrated in Fig. 15b is repeatedly applied to set $\mathbf{s} := (1-\frac{1}{c})\mathbf{n} + \frac{1}{2c}(\mathbf{w}+\mathbf{e})$. The BB-coefficients marked as • remain unconstrained, as do those marked ∘ since they do not affect C^1-join of the sectors. We *initialize* $\mathbf{g}$ as follows.

- The central point $\mathbb{o}$ of $\mathbf{g}$ is the extraordinary point $\mathbb{o}$ of bi-4 cap; the remaining $5 + 9n$ free BB-coefficients: 5 marked •, $6n$ marked • and $3n$ marked ∘, form a set S.
- The coefficients in S are set to minimize the sum of squared distances $|\mathbf{a}^s_{ij} - \tilde{\mathbf{a}}^s_{ij}|^2$ for all i, j and sectors s, where $\mathbf{a}^s := H^5(\mathbf{g}^s \circ \tau^s)$ are auxiliary bi-5 patches and $\tilde{\mathbf{a}}^s$ is the s-th sector of the bi-4 cap of Section 4, degree-elevated to bi-5.

6.2. *L-shaped tensor-borders form contracting rings*

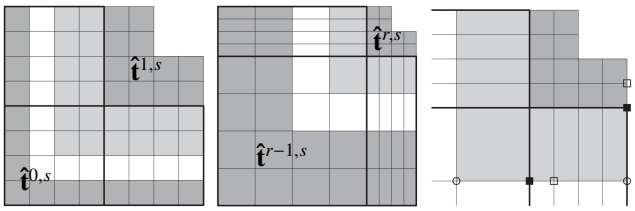

(a) $\sigma := \frac{1}{2}$ (b) $\sigma := \frac{3}{4}$ (c) C^1 extension

Figure 16: Construction of $\hat{\mathbf{p}}^{r,s}$ of degree bi-4 by merging the tensor-borders $\hat{\mathbf{t}}^{r-1,s}$ and $\hat{\mathbf{t}}^{r,s}$. (a) For $r = 1$, $\hat{\mathbf{t}}^{0,s}$ (dark gray) is the input tensor-border $\mathbf{t}^s$, degree-raised and split. The ring $\hat{\mathbf{p}}^{1,s}$ is assembled from $\hat{\mathbf{t}}^{0,s}$ and the uniform backwards C^2-extension (light-gray) of $\hat{\mathbf{t}}^{1,s}$. (b) For $r > 1$, dark-gray represents $\hat{\mathbf{t}}^{r-1,s}$ (split) and light-gray the backwards C^1-extension of $\hat{\mathbf{t}}^{r,s}$. (c) Enlargement of the backward C^1-extension.

The L-shaped tensor-borders $H^4(\mathbf{g} \circ \tilde{\chi}_\sigma)$ (see Fig. 6c) vary with σ and are the same for each (diagonally symmetric) sector. Therefore they can be implemented as a multiplication with a pre-calculated matrix, expressing the BB-coefficients of

the sampled tensor-borders as affine combinations of 21 BB-coefficients of one sector of the guide. Given a maximal anticipated level ℓ of refinement, the guided rings $\hat{\mathbf{p}}^{r,s}$, $r = 1,\dots,\ell$ (where s labels the sectors) are assembled by merging the sampled tensor-borders $\hat{\mathbf{t}}^{r-1,s}$, $\hat{\mathbf{t}}^{r,s}$, see Fig. 16.

Algorithm.

(1) Choose a sequence of speeds $(\sigma_1, \sigma_2, \dots, \sigma_\ell)$.
(2) Set $\dot{\mathbf{g}}^{0,s} := \mathbf{g}^s$ and iterate $\dot{\mathbf{g}}^{r,s}(u,v) := \dot{\mathbf{g}}^{r-1,s}(\lambda_{\sigma_r} u, \lambda_{\sigma_r} v)$. Each iteration amounts to computing the BB-coefficients of $\dot{\mathbf{g}}^{r,s}$ by de Casteljau's algorithm, see e.g. [20].
(3) Due to λ_σ-scalability of $\tilde{\chi}_\sigma$, the tensor-borders $\hat{\mathbf{t}}^{r,s}$ can be obtained multiplying pre-calculated matrices to the coefficients of $\dot{\mathbf{g}}^{r,s}$, followed by C^2 correction.
(4) Fig. 16 shows $\hat{\mathbf{p}}^{r,s}$ constructed from consecutive tensor-borders $\hat{\mathbf{t}}^{r-1,s}$ and $\hat{\mathbf{t}}^{r,s}$.
   (a) For $r = 1$, see Fig. 16a, $\hat{\mathbf{t}}^{0,s}$ is the degree-raised and evenly split input tensor-border $\mathbf{t}^s$. The first ring $\hat{\mathbf{p}}^{1,s}$ combines $\hat{\mathbf{t}}^{0,s}$ with the uniform *backward* (towards the surrounding surface) C^2-extension of $\hat{\mathbf{t}}^{1,s}$.
   (b) For $r > 1$ (see Fig. 16b) $\hat{\mathbf{t}}^{r-1,s}$ is split in the ratio $\sigma_r : \tilde{\sigma}_r$ while $\hat{\mathbf{t}}^{r,s}$ is backward C^1-extended (towards $\hat{\mathbf{t}}^{r-1,s}$) by applying, in vertical and horizontal directions, the stencil
   $\circ := \frac{1}{1-\sigma_r}\,\blacksquare - \frac{\sigma_r}{1-\sigma_r}\,\square$ (see Fig. 16c).

Default sequence σ_r. Formally, σ_r can take any value in (0..1). For $n \le 8$ the sequence $(\frac{1}{2}, \frac{3}{4}, \frac{7}{8})$ performs well. The initial $\sigma_1 := \frac{1}{2}$ yields a stable transition and so allows doubling the contraction speed in the two remaining rings. The size of the remaining hole is then as for six steps with $\sigma := \frac{1}{2}$, the 'speed' of Catmull-Clark subdivision. For $n > 8$, $\sigma = \frac{7}{8}$ can cause unwanted oscillations in the highlight lines (see Fig. 25) so that the sequence $(\frac{1}{2}, \frac{3}{4}, \dots, \frac{3}{4})$ is recommended.

6.3. An efficient but inferior tiny cap with G^1 transition

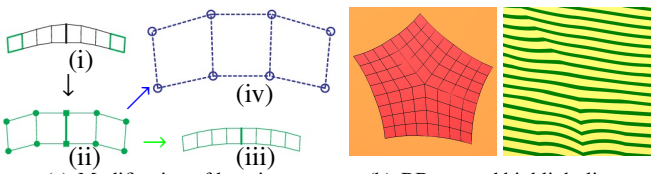

(a) Modification of last ring

(b) BB-net and highlight lines

Figure 17: The tiny cap with G^1 transition. (a) Modification of the last guided ring. (b) The BB-net of bi-4 cap and its highlight lines for the same configuration as in Fig. 2e.

Filling the remaining tiny hole with a G^1 bi-4 surface that preserves the good highlight line distribution of the guided bi-4 rings is surprisingly challenging. The simplest option, detailed in Fig. 17a, is to modify the last guided ring and apply the G^1 construction of Section 4:

(i) Convert the corner 2×2 jets of the last bi-4 tensor-border $\hat{\mathbf{t}}^\ell$ to bi-2 form $\bullet$ in (ii).
(ii) Join the jets C^1 to form the bi-2 tensor-border $\mathbf{t}$ by setting $\blacksquare$ as averages of neighboring $\bullet$.
(iii) Raise the degree of $\mathbf{t}$ to bi-4 and C^1-extend towards $\hat{\mathbf{t}}^{\ell-1}$.
(iv) Reverse the B-to-BB-conversion to obtain a DS-net from $\mathbf{t}$. The DS-net serves as input to the geometric bi-4 construction of Section 4.

However this simplest option introduces oscillations and propagates sharp highlight line transitions from the last ring into the tiny cap (see the zoom in Fig. 17b). We therefore build the tiny cap from 2×2 bi-4 macro-patches per sector and join the tiny cap C^1 to the last guided ring.

6.4. A superior tiny cap with C^1 transition

The cap $\hat{\mathbf{p}}$ is derived by pre-solving the G^1-constraints between the sectors, determining a planar parameterization $\hat{\tau}$ with the same layout and continuities as the tiny cap and constructing an auxiliary guiding cap $\mathbf{p}^{aux}$ by sampling jets of the guide $\mathbf{g}$ composed with $\hat{\tau}$. Then $\hat{\mathbf{p}}$ is a least-squares fit to $\mathbf{p}^{aux}$ and so as to satisfy all smoothness constraints.

G^1-constraints between the sectors. With the u- and v-directions as in the main construction (see Fig. 12) the constraints (3)

$$\partial_v \grave{\mathbf{p}} = a\partial_v \acute{\mathbf{p}} + b\partial_u \acute{\mathbf{p}},\ a(u) := -1,\ b(u) := 2\mathsf{c}(1-u) + \frac{2\mathsf{c}}{3}u,$$
$$\partial_v \underline{\grave{\mathbf{p}}} = \underline{a}\partial_v \underline{\acute{\mathbf{p}}} + \underline{b}\partial_u \underline{\acute{\mathbf{p}}},\ \underline{a}(u) := -1,\ \underline{b}(u) := \frac{2\mathsf{c}}{3}(1-u)^2, \qquad (14)$$

can be solved as

$$\acute{\mathbf{p}}_{i0} := \grave{\mathbf{p}}_{i0}, \underline{\acute{\mathbf{p}}}_{i0} := \underline{\grave{\mathbf{p}}}_{i0},\ i = 0,\dots,4;$$
$$\acute{\mathbf{p}}_{01} := \grave{\mathbf{p}}_{01} + 2\mathsf{c}\grave{\mathbf{p}}_{10} + 2(1-\mathsf{c})\grave{\mathbf{p}}_{00};$$
$$\grave{\mathbf{p}}_{20} := \frac{1}{9\mathsf{c}}(\mathsf{c}\grave{\mathbf{p}}_{00} + 4(2\mathsf{c}-3)\grave{\mathbf{p}}_{10} + 6(\grave{\mathbf{p}}_{11} + \acute{\mathbf{p}}_{11}));$$
$$\acute{\mathbf{p}}_{i1} := 2\grave{\mathbf{p}}_{i0} - \grave{\mathbf{p}}_{i1} + \frac{1}{4}\mathbf{f}_i,\ i = 2,3,4, \quad [\mathbf{f}_0,\dots,\mathbf{f}_4] \sim b(u)\partial_u \grave{\mathbf{p}};$$
$$\underline{\grave{\mathbf{p}}}_{0j} := \grave{\mathbf{p}}_{4j},\ \underline{\acute{\mathbf{p}}}_{0j} := \acute{\mathbf{p}}_{4j}, \quad \text{(join top and bottom } C^1\text{)}$$
$$\underline{\grave{\mathbf{p}}}_{1j} := 2\grave{\mathbf{p}}_{4j} - \grave{\mathbf{p}}_{3j},\ \underline{\acute{\mathbf{p}}}_{1j} := 2\acute{\mathbf{p}}_{4j} - \acute{\mathbf{p}}_{3j}, \quad j = 0,1$$
$$\underline{\grave{\mathbf{p}}}_{i0} := \frac{\underline{\grave{\mathbf{p}}}_{i1} + \underline{\acute{\mathbf{p}}}_{i1}}{2},\ i = 3,4 \quad (C^1 \text{ consistent with last ring})$$
$$\underline{\grave{\mathbf{p}}}_{20} := \frac{-1}{6}(\underline{\grave{\mathbf{p}}}_{00} + \underline{\grave{\mathbf{p}}}_{40}) + \frac{2}{3}(\underline{\grave{\mathbf{p}}}_{10} + \underline{\grave{\mathbf{p}}}_{30});$$
$$\underline{\acute{\mathbf{p}}}_{21} := 2\underline{\grave{\mathbf{p}}}_{20} - \underline{\grave{\mathbf{p}}}_{21} + \frac{1}{4}\mathbf{f}_2, \quad [\mathbf{f}_0,\dots,\mathbf{f}_4] \sim \underline{b}(u)\partial_u \underline{\grave{\mathbf{p}}};$$
$$\grave{\mathbf{p}}_{30} := \frac{1}{20}(6\grave{\mathbf{p}}_{20} + 17\grave{\mathbf{p}}_{40} - 4\underline{\grave{\mathbf{p}}}_{30} + \underline{\grave{\mathbf{p}}}_{40})$$

leaving unconstrained the BB-coefficients marked $\bullet$ and $\blacksquare$ in Fig. 18a. Here the linear $b(u)$ and the quadratic $\underline{b}(u)$ are C^1-connected and the sector-separating curve with coefficients $\underline{\grave{\mathbf{p}}}_{i0}$, $i = 0,\dots,4$ is of actual degree 3 (due to the assignment $\underline{\grave{\mathbf{p}}}_{20}$); and it is C^2-connected (due to assignment $\grave{\mathbf{p}}_{30}$) to the adjacent sector-separating curve with coefficients $\grave{\mathbf{p}}_{i0}$, $i = 0,\dots,4$.

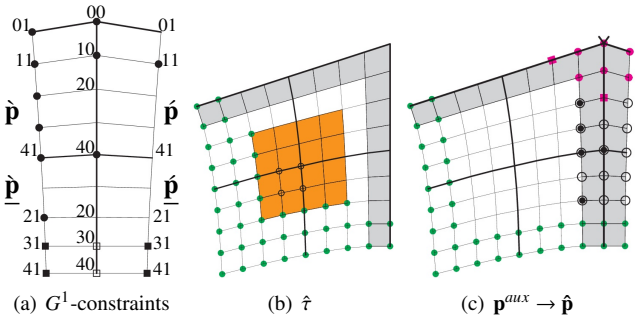

(a) G^1-constraints (b) $\hat{\tau}$ (c) $\mathbf{p}^{aux} \to \hat{\mathbf{p}}$

Figure 18: Tiny G^1 cap, C^1-connected to the last sampled ring. (a) G^1-constraints between sectors. (b) Parameterization $\hat{\tau}$. (c) Derivation of the central cap $\hat{\mathbf{p}}$ from the auxiliary cap $\mathbf{p}^{aux}$.

The 2×2 *parameterization* $\hat{\tau}$. In Fig. 18b, the BB-coefficients of the gray strips are set to enforce G^1-constraints between adjacent sectors and the BB-coefficients marked • represent evenly split, partly second-order tensor-borders $\tilde{\chi}_{\sigma_\ell}$. The four BB-coefficients, marked ∘, are unconstrained and define the remaining orange-underlaid BB-coefficients so that the four orange-underlaid 3×3 BB-nets join C^2. The diagonally symmetric, unbiased construction leaves free 10 scalars that are fixed to minimize the functional $\mathcal{F}_4$, see (1), over all four patches of the sector.

Choosing partly second-order Hermite data from the tensor-border $\tilde{\chi}_{\sigma_\ell}$ and joining the orange-underlaid BB-nets C^2 represents a *geometric* heuristic to evenly distribute BB-coefficients of $\hat{\tau}$ and so reduce the number of parameters to be set by $\mathcal{F}_4$.

A map $\mathbf{p}^{aux}$ is constructed by assembling the auxiliary 2×2 bi-4 per cap $H^4(\dot{\mathbf{g}}^\ell \circ \hat{\tau})$ per sector and replacing its BB-coefficients, marked • in Fig. 18c by BB-coefficients of the evenly split tensor-border $\hat{\mathbf{t}}^\ell$.

Then the *tiny cap* $\hat{\mathbf{p}}$ inherits the BB-net of $\mathbf{p}^{aux}$ except that ■ and the 14 BB-coefficients ∘ are replaced by the G^1-solution of (14) and the 5 unconstrained coefficients • are set to minimize the sum of squared distances between the BB-coefficients of $\hat{\mathbf{p}}$ and $\mathbf{p}^{aux}$ at the 14 locations ∘.

The last step can be efficiently implemented as multiplication with a pre-calculated 5×14 matrix.

6.5. *The superior tiny cap is flexibly* G^1*-refinable*

The tiny cap refines like the main construction in Section 5: the internal C^1 refinement is identical, the outer refinement is simpler since it is the C^1-extension of the C^1-refined last guided ring, and the refinement along the sector-separating curves only differs slightly from the main construction.

The tiny cap uses the layout of the once-refined main construction, see Fig. 14a, and the linear $b^0(u) := b(u)$ and quadratic $b^1(u) := \underline{b}(u)$ are split into $b^k(u)$ as in Section 5, i.e. so that by (6)

$$\acute{\mathbf{p}}_{i1} := 2\grave{\mathbf{p}}_{i0} - \grave{\mathbf{p}}_{i1} + \frac{1}{4}\mathbf{f}_i, i = 0, \dots, 4, \quad [\mathbf{f}_0, \dots, \mathbf{f}_4] \sim b^k(u)\partial_u \grave{\mathbf{p}}.$$

That is, the sector-separating curves closer to $\mathbb{m}^s$ are of actual degree 3 and their $b^k(u)$ of degree 2 so that Lemma 5 holds. For the sector-separating curves closer to $\mathbb{o}$, the $b^k(u)$ are linear and the refinement is structurally the same as in Section 5: the magenta ∘ BB-coefficients in Fig. 19a stem from a quadratic map $\tilde{\mathbf{q}}$ (obtained from the magenta BB-coefficients of the tiny cap by reversing the formula (12) with $\kappa := \hat{\kappa} := \frac{6+5c}{12(1+c)}$). Then with $\kappa := \hat{\kappa}$, Eq. (12) applies and the refinement of the quadratic expansion follows Section 5.1.

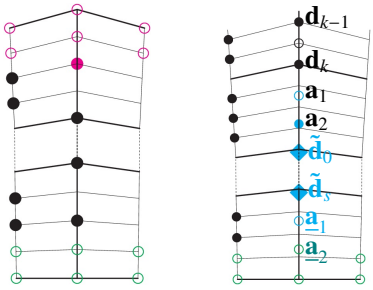

(a) main bi-4 (b) tiny bi-4

Figure 19: Structure of the G^1-refinement along a sector-separating curve.

Fig. 19b illustrates the refined uniform C^2 spline sector-separating curve from $\mathbb{m}^s$ to just beyond the spline control point $\mathbf{d}_k$ half ways to $\mathbb{o}$. At $\mathbf{d}_k$ the degree of the sector-separating curve switches from 4 to 3: $\mathbf{d}_{k-1}$ and $\mathbf{d}_k$ are B-spline control points of a degree 4 spline C^2-joined to a degree 3 spline using the stencil of Fig. 7b: $\mathbf{a}_1 := \frac{1}{5}(-2\mathbf{d}_{k-1} + 6\mathbf{d}_k + \mathbf{a}_2)$; and setting $\mathbf{a}_2 := \frac{1}{9}(-2\mathbf{d}_{k-1} + 6\mathbf{d}_k + 5\tilde{\mathbf{d}}_0)$ yields $\tilde{\mathbf{d}}_0 = 2\mathbf{a}_2 - \mathbf{a}_1$ so that $\tilde{\mathbf{d}}_0$ is a free B-spline control point of a uniform degree 3 spline.

Representing the C^1-extension of the last bi-4 ring in degree 3 form (see ∘) and choosing $\underline{\mathbf{a}}_1 := \frac{1}{2}(\underline{\mathbf{a}}_2 + \tilde{\mathbf{d}}_s)$ leaves $\tilde{\mathbf{d}}_s$ as a free B-spline control point of a degree 3 spline so that the degree 3 C^2 B-spline from $\mathbb{m}^s$ to $\mathbf{d}_k$ has the elegant standard sequence of B-spline control points. (Univariate B-to-BB conversion yields the BB-coefficients.)

In summary, the refined tiny cap is defined by

(a) independent control points of the surrounding bi-4 C^1-spline ring;
(b) independent BB-coefficients internal to (not in the two boundary layers of) each bi-4 C^1-spline macro-patch;
(c) six control points of the quadratic map at the extraordinary point $\mathbb{o}$;
(d) independent control points of a C^2-spline sector-separating curve with
  - $\mathbf{d}_j$ of degree 4 (and not defined by (c)),
  - $\tilde{\mathbf{d}}_i$ of degree 3; and
(e) independent control points, marked • in Fig. 19b, of a C^1-spline of degree 4 (and not defined by (a) nor (c)).

Similarly as in Section 5.2, we can define the associated basis functions and prove their linear independence.

7. Examples

The input net of Fig. 20a can define a C^1 surface ring of $2n = 6$ bi-2 patches. This bi-2 ring is colored green in Fig. 20b while

the bi-4 cap Section 4 is red. Fig. 20c shows the alternative sequence of guided rings with default speeds $(\frac{1}{2}, \frac{3}{4}, \frac{7}{8})$ and a tiny central cap, so small that one could opt for just two rings. The highlight line distribution of the alternative construction as well as at the tiny cap, shows no blemish, and is visually identical to that of the default construction of Section 4.2

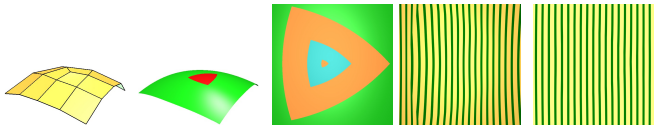

(a) $n = 3$ net (b) default (c) alternative layout (d) near cap

Figure 20: Bi-4 constructions for $n = 3$: (b) default of Section 4.2 and (c) alternative layout. (d) highlight lines of the alternative layout near the tiny cap.

The color conventions of Fig. 20 are applied to all following surfaces.

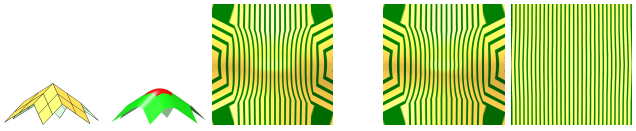

(a) $n = 6$ (b) default (c) alternative

Figure 21: Bi-4 constructions for $n = 6$. (a) Input net. (b) default bi-4 construction and highlight lines of the multi-sided surface. (c) Alternative guided hybrid: highlight lines as in (b) and zoomed in on the tiny cap.

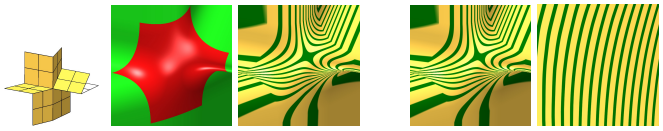

(a) $n = 7$ (b) default (c) alternative

Figure 22: Bi-4 constructions for $n = 7$. (b) Default construction. (c) Alternative guided hybrid: highlight lines from far and enlarged to focus on the tiny cap.

The convex $n = 6$ net of Fig. 21a yields uniformly-spaced highlight lines across the caps, and the same can be said about the three-beam input net of Fig. 22. Remarkably, the zoom focused on the neighborhood of the tiny cap, betrays neither the C^1 transitions between the guided rings nor the G^1 transitions of the tiny cap.

Fig. 23 displays the alternative surface with various tiny caps for $n = 8$ net. In the view of Fig. 23b the caps look alike; only by zooming into area of tiny cap Fig. 23c shows the differences. The G^1 transition Fig. 23d is clearly worse and artifacts increase with valence (compare to Fig. 17b).

Fig. 24 demonstrates good quality also for exotic shapes and valencies. Fig. 24c illustrates how portions of BB-net can be manipulated freely in the subdivision part of the alternative construction. Similar editing of the default G^1-refinable construction would be very cumbersome.

Fig. 25 demonstrates that the speed sequence $(\frac{1}{2}, \frac{3}{4}, \frac{7}{8})$, that works very well for the common valences $n = 3, 5, 6$ and up to

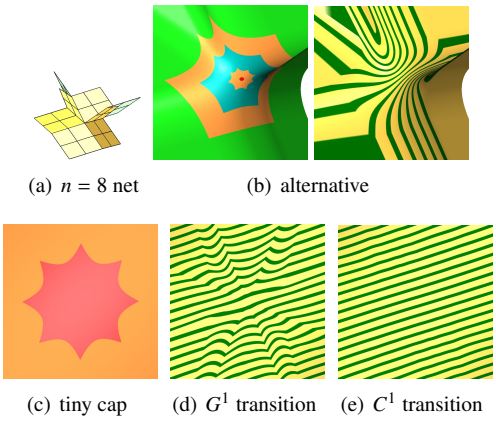

(a) $n = 8$ net (b) alternative

(c) tiny cap (d) G^1 transition (e) C^1 transition

Figure 23: Guided rings plus tiny cap hybrid for $n = 8$. *bottom*: highlight lines of alternative tiny caps.

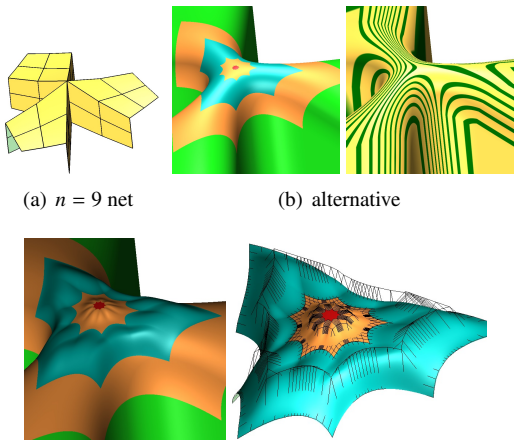

(a) $n = 9$ net (b) alternative

(c) localized design

Figure 24: Guided plus tiny cap construction for $n = 9$ with local edits.

$n = 8$, can yield unwanted oscillations of highlight lines for very high valencies, here $n = 10$, in the narrow area along the sector-separating curve for $\sigma = \frac{7}{8}$. In Fig. 25c, ↓ points to one such spot. The oscillations disappear for the sequence $(\frac{1}{2}, \frac{3}{4}, \frac{3}{4}, \frac{3}{4})$, see Fig. 25d.

8. Conclusion

The curious phenomenon that refined control nets of generalized spline surfaces fail to offer additional degrees of freedom for modelling or engineering analysis along certain curves was shown to be the result of the G^1 constraints combined with low degree. In particular, Theorem 1 proved that G^1 refinement of symmetric, unbiased, multi-sided bi-3 G^1 surfaces with internally C^1 sectors, suitable for inclusion into C^1 bi-2 splines, does not increase flexibility along the sector-separating curves or input boundary.

On the constructive side, an explicit multi-sided bi-4 spline surface exhibits good highlight line distributions and was proven to be flexibly G^1-refinable. This solution was complemented by an alternative hybrid construction that supports re-

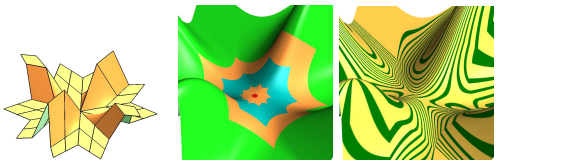

(a) $n = 10$ net (b) alternative, $(\frac{1}{2}, \frac{3}{4}, \frac{7}{8})$

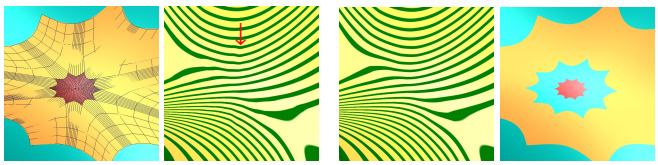

(c) $(\frac{1}{2}, \frac{3}{4}, \frac{7}{8})$, last ring + cap (d) $(\frac{1}{2}, \frac{3}{4}, \frac{3}{4}, \frac{3}{4})$, last two rings + cap

Figure 25: Comparison of different speed sequences for $n = 10$. (b) Speed sequence $(\frac{1}{2}, \frac{3}{4}, \frac{7}{8})$: layout and highlight lines. (c) The last guided ring and tiny cap with overlaid BB-nets. (d) Speed sequence $(\frac{1}{2}, \frac{3}{4}, \frac{3}{4}, \frac{3}{4})$: the last two guided rings plus tiny cap.

finement with simpler C^1 transitions, except inside a final tiny cap. This hybrid has uniformly distributed degrees of freedom along the sector-separating curves and is flexibly G^1-refinable as is desirable for engineering analysis and editing fine geometric details.

Acknowledgements. This work was supported in part by DARPA HR00111720031 and NIH R01 EB018625.

[1] D. Doo, M. Sabin, Behaviour of recursive division surfaces near extraordinary points, Computer-Aided Design 10 (1978) 356–360.
[2] E. Catmull, J. Clark, Recursively generated B-spline surfaces on arbitrary topological meshes, Computer-Aided Design 10 (1978) 350–355.
[3] D. Groisser, J. Peters, Matched G^k-constructions always yield C^k-continuous isogeometric elements, Computer Aided Geometric Design 34 (2015) 67–72.
[4] K. Karčiauskas, J. Peters, Smooth multi-sided blending of biquadratic splines, Computers & Graphics 46 (2015) 172–185.
[5] K.-P. Beier, Y. Chen, Highlight-line algorithm for realtime surface-quality assessment, Comp-Aid Design 26 (4) (1994) 268–277.
[6] K. Karčiauskas, J. Peters, A sharp degree bound on G^2-refinable multi-sided surfaces, CAD to appear (2020) 1–12, jCAD 102867. doi:https://doi.org/10.1016/j.cad.2020.102867.
[7] K. Karčiauskas, J. Peters, Refinable smooth surfaces for locally quad-dominant meshes with T-gons, Computers& Graphics 82 (2019) 193–202.
[8] U. Reif, Biquadratic G-spline surfaces, Computer Aided Geometric Design 12 (2) (1995) 193–205.
[9] C. Loop, T. DeRose, Generalized B-spline surfaces of arbitrary topology, in: F. Baskett (Ed.), Computer Graphics (SIGGRAPH '90 Proceedings), Vol. 24, ACM, 1990, pp. 347–356.
[10] J. Deng, F. Chen, L. Jin, Dimensions of biquadratic spline spaces over t-meshes, J. Computational Applied Mathematics 238 (2013) 68–94.
[11] C. Zeng, F. Deng, X. Li, J. Deng, Dimensions of biquadratic and bicubic spline spaces over hierarchical t-meshes, J. Computational Applied Mathematics 287 (2015) 162–178.
[12] K. Karčiauskas, J. Peters, Point-augmented biquadratic C^1 subdivision surfaces, Graphical Models 77 (2015) 18–26.
[13] G. Farin, Curves and Surfaces for Computer Aided Geometric Design: A Practical Guide, Academic Press, 1988.
[14] C. de Boor, A Practical Guide to Splines, Springer, 1978.
[15] K. Karčiauskas, J. Peters, Adjustable speed surface subdivision, Computer Aided Geometric Design. 26 (2009) 962–969.
[16] A. Collin, G. Sangalli, T. Takacs, Analysis-suitable G^1 multi-patch parametrizations for C^1 isogeometric spaces, Computer Aided Geometric Design 47 (2016) 93–113.
[17] P. Alfeld, L. Schumaker, The dimension of bivariate spline spaces of smoothness r and degree $d \geq 4r+1$, Constructive Approximation 3 (1987) 189–197.
[18] M.-J. Lai, L. L. Schumaker, Spline functions on triangulations, Vol. 110 of Encyclopedia of mathematics and its applications, Cambridge University Press, 2007.
[19] B. Mourrain, On the dimension of spline spaces on planar t-meshes, Math. Comput 83 (286).
[20] K. Karčiauskas, J. Peters, Fair free-form surfaces that are almost everywhere parametrically C^2, Journal of Computational and Applied Mathematics (2018) 1–10.

Appendix: Proof of Proposition 1

For completeness, this section adapts the argument of [6, Appendix C] to the G^1 case. The argument uses (R): If f is a polynomial and g is a rational, then $h = f + g$ is rational.

Lemma 6 (along $\mathbb{c}^s, \mathbb{m}^s$). *If the BB-coefficients $\mathbf{t}_{ij}$ of the tensor-border $\mathbf{t}$ can be independently chosen and if both $\mathbf{t}$ and $\tilde{\mathbf{t}} := \mathbf{t} \circ \rho$ are polynomial, then the scalar functions a, b defining ρ in (3) are polynomials.*

Proof For $\deg(\mathbf{t}) = m$, the G^1 constraints (3) can be written as

$$\partial_v \tilde{\mathbf{t}}(u,0) = \underbrace{\sum_i a(u) B_i^m(u) m \mathbf{t}_{i1}}_{E_1(u)} - \underbrace{\sum_i a(u) B_i^m(u) m \mathbf{t}_{i0}}_{E_2(u)} + \underbrace{\sum_i b(u) (B_i^m(u))' m \mathbf{t}_{i0}}_{E_3(u)}$$

If we set all $\mathbf{t}_{ij}$ to zero except one $\mathbf{t}_{i1}$ for fixed i then the G^1 constraints (3) simplify to $\partial_v \tilde{\mathbf{t}}(u,0) = a(u) B_i^m(u) m \mathbf{t}_{i1}$ implying that $a(u) B_i^m(u)$ is a polynomial. If $a(u) := \frac{\bar{a}(u)}{\underline{a}(u)}$ is rational then the denominator $\underline{a}(u)$ must be a factor of $B_i^m(u)$ for all i. Since the gcd of the Bernstein polynomials is 1, this implies that $a(u)$ is a polynomial.

Since now $\partial_v \tilde{\mathbf{t}}(u,0) - E_1(u) + E_2(u)$ is a polynomial, by (R) so is $E_3(u)$, and by setting all $\mathbf{t}_{ij}$ to zero except for one $\mathbf{t}_{i0}$ for fixed i, we see that $b(u)(B_i^m(u))'$ must be polynomial for each i. Since the gcd of the $(B_i^m(u))' = \binom{m}{i}(1-u)^{m-1-i} u^{i-1}(i - mu)$ is 1, $b(u)$ must be a polynomial. |||

Now consider the sector-separating curves.

Lemma 7 (along $\mathbb{m}^s, \mathbb{o}$). *If both $\grave{\mathbf{p}}$ and $\acute{\mathbf{p}} := \grave{\mathbf{p}} \circ \rho$ are polynomial, and $a(u)$ in $\rho(u,v) := (u + b(u)v, a(u)v)$ is polynomial then $b(u)$, too, is polynomial.*

Proof Applying (R) to the G^1 constraint $\partial_v \acute{\mathbf{p}} := a\, \partial_v \grave{\mathbf{p}} + b\, \partial_u \grave{\mathbf{p}}$ when $a(u)$ is polynomial implies that $b(u) \partial_u \grave{\mathbf{p}}(u,0)$ is polynomial. Presenting $\grave{\mathbf{p}}(u,0)$ in BB-form of least degree (sector-separating curves may be of lower degree than the patches that join) and setting the corresponding independent coefficient of $\partial_u \grave{\mathbf{p}}(u,0)$ to zero except for one, we conclude as in Lemma 6 that the denominator of $b(u)$ must be 1. |||

Proof of Proposition 1. B-to-BB conversion transforms the 3×2 independently choosable control points of the surrounding

bi-2 B-spline to 3×2 independently choosable BB-coefficients of the tensor-border $\mathbf{t}$, see Fig. 3b. Therefore Lemma 6 proves claim (i); and since no bias implies $a(u) \equiv -1$, Lemma 7 proves claim (ii).